Anomalous scaling and breakdown of conventional density functional theory methods for the description of Mott phenomena and stretched bonds

Zu-Jian Ying,[1,2,*] Valentina Brosco,[1,†] Giorgia Maria Lopez,[3] Daniele Varsano,[4] Paola Gori-Giorgi,[5] and José Lorenzana[1]

[1]*ISC-CNR and Dipartimento di Fisica, Università di Roma "La Sapienza," Piazzale Aldo Moro 2, 00185 Roma, Italy*

[2]*Beijing Computational Science Research Center, Beijing 100084, China*

[3]*CNR-IOM, Istituto Officina dei Materiali, Cittadella Universitaria, Monserrato (CA) 09042, Italy*

[4]*Center S3, CNR Institute of Nanoscience, Via Campi 213/A, 41125 Modena, Italy*

[5]*Department of Theoretical Chemistry and Amsterdam Center for Multiscale Modeling, FEW, Vrije Universiteit Amsterdam, Amsterdam 1081 HV, Netherlands*

(Received 17 June 2016; published 29 August 2016)

Density functional theory provides the most widespread framework for the realistic description of the electronic structure of solids, but the description of strongly correlated systems has remained so far elusive. We consider a particular limit of electrons and ions in which a one-band description becomes exact all the way from the weakly correlated metallic regime to the strongly correlated Mott-Hubbard regime. We provide a necessary condition a density functional should fulfill to describe Mott-Hubbard behavior in this one-band limit and show that it is not satisfied by standard and widely used local, semilocal, and hybrid functionals. We illustrate the condition in the case of few-atom systems and provide an analytic approximation to the exact exchange-correlation potential based on a variational wave function which shows explicitly the correct behavior, combining in a neat way lattice and continuum methods.

DOI: 10.1103/PhysRevB.94.075154

I. INTRODUCTION

Density functional theory (DFT) plays a fundamental role to understand matter around us [1]. In the last 30 years, approximate functionals have increased in complexity and accuracy. The local density approximation (LDA) proposed in the original paper [2] by Kohn and Sham (KS) is already rather accurate for many solids. With the advent of generalized gradient approximations (GGA) [3,4] and hybrid functionals [5], DFT became the workhorse in computational chemistry also. More sophisticated semilocal functionals are the meta-GGAs that using the KS kinetic energy density as input can recognize different types of bonds [6,7], can provide accurate potentials in asymptotic regions [8,9], and even can detect excitonic effects in semiconductors [10]. However, current DFT implementations fail to describe the correlation-induced suppression of tunneling of electrons encountered in materials with d or f open shells which, as first discussed by Mott [11], may lead to insulating behavior and affect deeply the thermodynamics and ground-state properties of correlated metals close to the Mott phase [12] and so-called heavy fermions [13,14].

Sometimes allowing for a spin-density-wave broken-symmetry solution within spin DFT provides a good ground-state description of magnetic insulators. While this is a popular way out, even for molecules that have a singlet ground state, it has several unwanted features, the more fundamental one being that for the case of the H_2 molecule it is known that the exact Kohn-Sham solution does not show such broken symmetry at any distance [15,16]. Even if one neglects that, practical problems appear. For example, spurious crossings of solutions as the molecule is stretched [17] spoil molecular dynamics computations. Furthermore, in the case of correlated metals that do not have a broken-symmetry ground state as heavy fermions [13] or slightly doped cuprates [18], artificially broken-symmetry solutions would lead to the wrong volume of the Fermi surface apparently violating Luttinger theorem [19]. Thus, it is highly desirable to overcome the deficiencies of current DFT methods without allowing for such broken-symmetry solutions.

It is commonly believed that such problems "cannot be remedied by using more complicated exchange-correlation functionals in DFT" (see Ref. [20]). Instead, these effects have been successfully described by means of lattice models, such as the Hubbard model [21–23], employing a series of techniques which have evolved into modern dynamical mean-field theory (DMFT) [24]. This led to intense efforts to combine lattice and DFT methods [20,25–29].

In this work, we derive a necessary condition a functional should satisfy to be able to describe Mott-Hubbard behavior in a band that can be described both by the continuum and a one-band Hubbard model. We show that most functionals in use today in chemistry and physics, including local, semilocal, and hybrid functionals [30], do not satisfy the condition and they cannot describe Mott-Hubbard phenomena. The problem becomes evident by examining how functionals behave under a rescaling of the length units. This provides a rigorous ground to the quoted statement of Ref. [20] when restrained to conventional approximations. Here, by "conventional" we refer broadly to any functional whose exchange-correlation (xc) potential converges to an exchangelike contribution in the high-density limit.

We also obtain numerically the behavior of the xc potential in simple test cases that can be treated with accurate wave-function methods. We show that a suitable analytical

*Present address: CNR-SPIN, and Dipartimento di Fisica "E. R. Caianiello," Università di Salerno, I-84084, Fisciano (Salerno), Italy.

†Present address: Istituto Officina dei Materiali (IOM) and Scuola Internazionale Superiore di Studi Avanzati (SISSA), Via Bonomea 265, 34136 Trieste, Italy.

combination of DFT and lattice methods captures the correct behavior with surprising good accuracy.

II. CONTINUUM MODEL AND ONE-BAND LIMIT

We first define a limit where the continuum model of electrons in a periodic potential $v_{\rm ext}$ and a generalized one-band Hubbard model are bound to provide quantitatively equivalent solutions. We consider N electrons moving in the potential $v_{\rm ext}$ produced by a collection of N identical nuclei of charge Ze located on the sites $\tilde{\mathbf{R}}_i$ of a periodic lattice with spacing $\tilde{a}$. The Hamiltonian in atomic units reads as

$$\tilde{H} = -\frac{1}{2}\sum_{i}^{N}\nabla^2_{\tilde{\mathbf{r}}_i} - \sum_{ij}^{N}\frac{Z}{|\tilde{\mathbf{r}}_i - \tilde{\mathbf{R}}_j|} + \frac{1}{2}\sum_{i\neq j}^{N}\frac{1}{|\tilde{\mathbf{r}}_i - \tilde{\mathbf{r}}_j|}, \quad (1)$$

where $\tilde{\mathbf{r}}_i$ are the electron coordinates. The system can be viewed as a half-filled $1s$ band in which the atomic number Z controls the orbital size $a_{\rm B}/Z$, with $a_{\rm B}$ the Bohr radius.

In the following, quantities without tilde are expressed in "scaled units" in which the orbital size is the unit of length, i.e.,

$$a = Z\frac{\tilde{a}}{a_B}, \quad (2)$$

and Z^2 Ha is the unit of energy. In these units, the Hamiltonian reads as

$$H = \sum_{i}^{N}\hat{h}(\mathbf{r}_i) + \frac{1}{2Z}\sum_{i\neq j}^{N}\frac{1}{|\mathbf{r}_i - \mathbf{r}_j|}, \quad (3)$$

where $\hat{h}(\mathbf{r})$ is the one-body Hamiltonian, $\hat{h}(\mathbf{r}) = -\frac{1}{2}\nabla^2_{\mathbf{r}} + v_{\rm ext}(\mathbf{r})$ with

$$v_{\rm ext}(\mathbf{r}) = -\sum_{j}^{N}\frac{1}{|\mathbf{r} - \mathbf{R}_j|}.$$

Notice that, in rescaled units, the one-body part becomes Z independent and $1/Z$ plays the role of a coupling constant [31]. We will use a and Z as our control variables.

Our first goal is to define a region of the parameter space (a, Z), where a one-band lattice model describes not only qualitatively but also quantitatively the continuum model defined by Eq. (3) (hereafter "the one-band limit"). As it is well known from studies of the Hubbard model [21–24,32–35], the most important energy scales in this problem are the Hubbard onsite interaction U and the nearest-neighbor hopping matrix element t, which define the weakly correlated regime $0 < U \ll zt$, and the strongly correlated regime $U \gg zt$, with z denoting the lattice coordination.

For hydrogen ($Z = 1$), the elimination of higher-energy bands is inaccurate since the energy cost [36] $U = 0.47$ Ha of a charge fluctuation $1s^1 1s^1 \to 1s^0 1s^2$ is similar to the cost $\Delta = \frac{3}{8}$ Ha of a charge fluctuation $1s^1 1s^1 \to 1s^1 2s^1$. This can be seen already in the atomic limit comparing the above "screened" Hubbard repulsion U (defined as the difference between ionization and affinity energy of hydrogen) with the "bare" Hubbard repulsion $U_0 = \frac{5}{8}$ Ha [obtained from Coulomb integrals, Eq. (A3)]. This difference is due to the effect of the higher orbitals which have to be taken into account in the model in order to provide a quantitative description. To avoid this problem, we take the limit of large Z so that $\Delta \sim Z^0 \gg U \sim 1/Z$. As can be seen from Fig. 1, as Z grows the screened U asymptotically approaches the bare U_0 showing that corrections from higher orbitals (at energy separation at least Δ) become irrelevant. In order to keep the system in the correlated regime of the Hubbard model in addition, we adjust $a \sim \ln(Z)$ so that $t/U \sim e^{-a}/(1/Z)$ is kept constant. In this limit, the condition

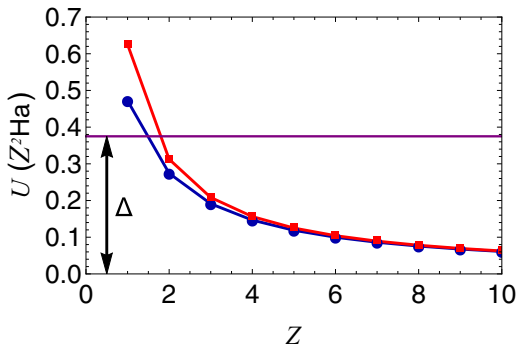

FIG. 1. Vanishing of screening effects at large atomic number in the atomic limit. The $1s$ Hubbard U is shown vs the atomic number. In red, we show the bare value U_0 from Coulomb integrals [Eq. (A3)], while the blue dots are the "screened" value obtained as $U = E_I^{Z,Z} - E_I^{Z,Z-1}$ where $E_I^{Z,n}$ is the nth ionization energy [36] for atomic number Z. ($E_I^{1,0} \equiv E_A$ is the affinity energy for hydrogen.) The horizontal line is the cost Δ of a charge fluctuation $1s^1 1s^1 \to 1s^1 2s^1$.

$$\Delta \gg t, U \quad (4)$$

is fulfilled allowing us to study quantitatively Mott-Hubbard phenomena in the model equation (3) from the weakly to the strongly correlated regime within a one-band description. Notice that the order of limits is important. The atomic limit of the one-band model is obtained by doing first $a/\ln(Z) \to \infty$ and then $Z \to \infty$, the other way around yields the noninteracting limit.

Our next goal is to determine how the xc potential scales with Z in the strongly correlated one-band limit. While the one-band simplification is rigorously valid in a many-body description, we will show below that it is forbidden in exact Kohn-Sham DFT.

A. Lattice model

In the one-band limit, the continuum model is equivalent to a generalized Hubbard model which can be obtained by the standard second-quantization procedure employing a single-particle basis of $1s$ orbitals $\phi_i(\mathbf{r})$ centered at $\mathbf{R}_i$ (see Appendix A and Refs. [21–23,37–39]). It will become clear below that our arguments are sufficiently general that are valid for such generalized Hubbard model. However, to fix ideas it is useful to think in terms of the standard Hubbard model [21–23] which can be obtained by absorbing the long-range part of the Coulomb interaction in mean field in the onsite

energy v and restricting the hopping to nearest neighbors $\langle ij\rangle$:

$$H_H = \sum_{i\sigma} v\, n_{i\sigma} - t \sum_{\langle ij\rangle\sigma} (c^\dagger_{i\sigma} c_{j\sigma} + \text{H.c.}) + U \sum_i n_{i\uparrow} n_{i\downarrow}, \tag{5}$$

with $c_{i\sigma}$ ($c^\dagger_{i\sigma}$) the annihilation (creation) operator for an electron with spin σ on site i and $n_{i\sigma} \equiv c^\dagger_{i\sigma} c_{i\sigma}$.

To link lattice and DFT descriptions, we need the correlated density which is determined by the one-body density matrix of the lattice model ($\rho_{ij} \equiv \sum_\sigma \langle c^\dagger_{j\sigma} c_{i\sigma}\rangle$) and the ϕ_i's (Appendix A). The density can be separated into an "atomic" component and a "bond-charge" contribution $n(\mathbf{r}) = n_{\text{at}}(\mathbf{r}) + n_{\text{bd}}(\mathbf{r})$ with

$$n_{\text{at}}(\mathbf{r}) = \sum_i |\phi_i(\mathbf{r})|^2 \rho_{ii}, \tag{6}$$

$$n_{\text{bd}}(\mathbf{r}) = \sum_{\langle ij\rangle} \phi^*_j(\mathbf{r}) \phi_i(\mathbf{r}) \rho_{ab} + \text{c.c.}, \tag{7}$$

where we have used the fact that for large a (one-band limit) the sums in Eq. (7) can be restricted to nearest neighbors and we have defined the nearest-neighbor density matrix element $\rho_{ij} = \rho_{ab}$. In our case, $\rho_{ii} = 1$, thus, all the dependence of the density on U/t is encoded in the bond charge and it is controlled by ρ_{ab}. For a large enough value of Z so that the one-band approximation is accurate, we can study the system from small to large U/t by either varying a or changing Z at a fixed a. In the latter case, since the ϕ_j's can be taken as fixed independently of the value of U/t, Eq. (7) establishes a one-to-one mapping between the density and ρ_{ab} as U/t (or equivalently Z) is varied.

Notice that because of the orthogonality of the Wannier wave functions $n_{\text{bd}}(\mathbf{r})$ integrates to zero and describes transfer of charge between the core atomic region and the bonds.

III. BREAKDOWN OF CONVENTIONAL DFT METHODS

A. Hartree approximation

We now go back to the continuum model. Before examining DFT, we analyze the ground state of Hamiltonian (3) in the Hartree approximation. As an initial guess of the Hartree orbitals, we can take the eigenstates of the noninteracting problem. We will show below that the Hartree potential $v_H(\mathbf{r})$ is at most of order $O(1/Z)$, thus, since Δ is $O(Z^0)$, the corrections to the initial guess can be neglected and, to leading order in $1/Z$, the Hartree orbitals coincide with the noninteracting orbitals and the Hartree self-consistent density coincides with the noninteracting density. To show this explicitly and fix ideas, let us consider the case $N = 2$, although the arguments are easily generalized to any N. The initial guess of the occupied Hartree orbital is the bonding state

$$\psi^{\text{H}}_0(\mathbf{r}) = \frac{1}{\sqrt{2}}[\phi_a(\mathbf{r}) + \phi_b(\mathbf{r})].$$

Here, $i = a,b$ labels the two ions and we assume real orbitals. The Hartree density is given by $n^H(\mathbf{r}) = 2|\psi^{\text{H}}_0(\mathbf{r})|^2$ or, equivalently, by Eqs. (6) and (7), inserting ρ_{ij} in the Hartree approximation ρ^H_{ij}, where for two sites $\rho^H_{ab} = 1$.

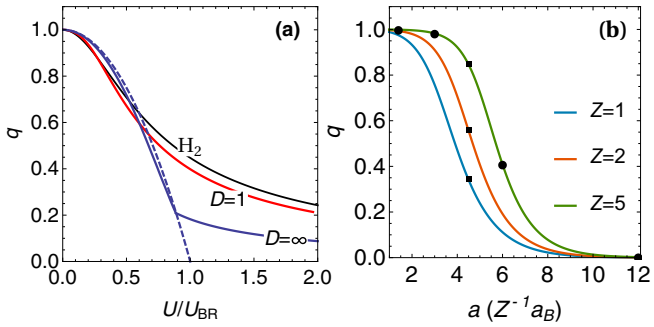

FIG. 2. Hopping reduction factor. (a) Exact results (full lines) as a function of U/U_{BR} for the Hubbard model in dimension D. Here, U_{BR} is a measure of the effective noninteracting bandwidth [40], $U_{\text{BR}} \equiv \frac{16}{N} \sum_{k\in\text{occ.}} \epsilon_k$ where ϵ_k are the single-particle noninteracting energies and the sum is restricted to the occupied states. We show results for a two-site system (black), for an infinite chain (red), and for the Bethe lattice in infinite dimensions (blue). The Bethe lattice data were derived from numerical [41] and analytic [42] results (full blue line). The cusp signals U_{c2} where the Mott-Hubbard transition occurs from the metallic phase ($U < U_{c2}$) to the insulating phase ($U > U_{c2}$). The dashed line was obtained with the Gutzwiller wave function for the same Bethe lattice. (b) Hopping reduction factor obtained with a Gutzwiller-type wave function in a hydrogenic molecule as a function of atom separation a for different atomic numbers. The dots (squares) correspond to the cases considered in Figs. 5(a) and 5(b) [Figs. 5(c), 5(d), and 3].

The Hartree potential is given by

$$v_H(\mathbf{r}) = \frac{1}{Z} \int d^3\mathbf{r}' \frac{n^H(\mathbf{r}')}{|\mathbf{r} - \mathbf{r}'|}.$$

This is finite everywhere and it has a maximum that scales at most as $1/Z$. Thus, we can always choose Z large enough so that $v_H/\Delta \sim 1/Z$ is small and the noninteracting orbitals coincide with the Hartree orbitals. We anticipate that while the same is valid in LDA, contrary to what can be expected on first sight, this is not any more valid for the exact Kohn-Sham xc potential.

B. How Mott-Hubbard correlations are encoded in the density

Since DFT provides an exact description [1], Mott-Hubbard behavior should be encoded in the density. In the one-band limit, this can only happen through the bond-charge equation (7) which can be parametrized through the hopping reduction factor defined as

$$q \equiv \frac{\rho_{ab}}{\rho^H_{ab}}. \tag{8}$$

For an interacting system, one typically finds $q < 1$. For example, Fig. 2(a) shows the hopping reduction factor of the Hubbard model for exactly solvable lattices. In more general cases, a good estimate of the hopping reduction factor can be obtained with a variational Gutzwiller wave function (see Appendix A 1). For the two-site Hubbard model, this yields the exact solution, while for infinite dimension it provides an accurate estimate in the metallic phase (dashed line in Fig. 2).

For the full model equation (A2), the qualitative behavior of the hopping reduction factor does not change as it can be

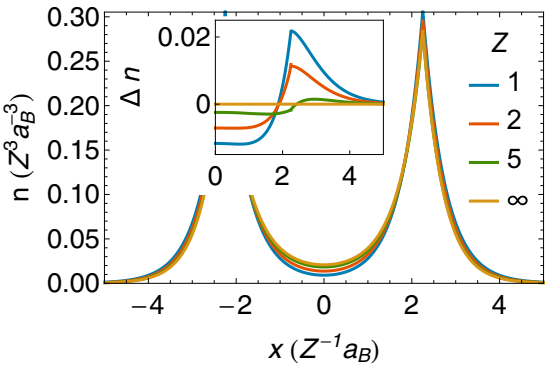

FIG. 3. Charge along the bond for interatomic distance $a = 4.5$ ($a_B Z^{-1}$) and various values of Z. The inset shows the interacting charge minus the noninteracting charge ($Z = \infty$). Charges where computed within full CI (see Appendix H).

easily checked using perturbation theory. Figure 2(b) shows the hopping reduction factor computed with a variational Gutzwiller-type wave function for the two-site full model (Appendix A 1) as a function of the interatomic distance a. Since t decreases exponentially with a, one obtains a rapid crossover from the weakly correlated regime ($q \sim 1$) to the strongly correlated regime ($q \sim 0$). (In the quantum chemistry literature, the latter is often referred to as the regime of "nondynamical" correlations.) It is believed that the crossover turns into the Mott metal-insulator transition in high-dimensional lattices as Fig. 2(a) suggests.

From the above discussion it is clear that in the one-band limit, independently of the dimensionality, the correlated charge in the bond is depleted with respect to a Hartree computation [cf. Eqs. (7) and (8) and Fig. 2]. Figure 3 shows an accurate computation of the density in scaled units and within the full configuration interaction (CI) approach as explained in Appendix H. For small Z (strong correlation), the bond charge is indeed depressed, however, the differences are minute which makes extremely challenging for DFT to be sensitive to Mott-Hubbard correlations.

C. Density functional theory

In Kohn-Sham theory [2], the interacting system is mapped into a system of noninteracting electrons moving in an effective potential which is the sum of the external potential, the Hartree (H) potential, and the xc potential:

$$v_{\mathrm{KS}}(\mathbf{r}) = v_{\mathrm{ext}}(\mathbf{r}) + v_{\mathrm{H}}(\mathbf{r}) + v_{\mathrm{xc}}(\mathbf{r}). \tag{9}$$

In the exact formulation, the noninteracting system reproduces the exact density of the interacting system, however, in practice v_{xc} is an unknown functional of the density and approximations are needed. In the local density approximation [2,30] (LDA), the xc potential is a simple function of the local density $v_{\mathrm{xc}}^{\mathrm{LDA}}(\mathbf{r}) = v_{\mathrm{xc}}^{\mathrm{LDA}}[n(\mathbf{r})]$. We show now that LDA cannot account for Mott-Hubbard correlations of the system.

To solve KS equations in LDA one can use again the Hartree density n^{H} as a starting guess. Using a standard parametrization of the potential, it is easy to show that $v_{\mathrm{Hxc}}^{\mathrm{LDA}}$ is at most of order $\sim 1/Z$ (see Appendix B). For large Z, the change in the orbitals is then of order $v_{\mathrm{Hxc}}^{\mathrm{LDA}}/\Delta \sim 1/Z$ and it can be neglected. Thus, in the one-band limit, LDA orbitals coincide with the Hartree orbitals and the density is given by Eqs. (6) and (7) with $\rho_{ij}^{\mathrm{LDA}} = \rho_{ij}^{H}$ independently of U/t. It is clear that LDA cannot account for the bond-charge reduction which is a primary characteristic of Mott-Hubbard correlations.

The failure of LDA can be traced back to the $1/Z$ scaling of v_{xc}. Clearly, the exact v_{xc} cannot scale as $1/Z$ everywhere since, if it did so, the same argument as for LDA would apply. The only way to generate the correlated density with a noninteracting system is by modifying the orbitals, and this can only happen by allowing the low-energy $1s$ states to be mixed with high-energy single-particle states outside the minimal basis set, consistently with the known fact that exact KS-DFT breaks down when restricted to a finite basis set [44,45].

For large Z, the mixing of the $1s$ band with the higher bands can only be achieved if the xc potential is of order Z^0. It follows that a necessary condition that a functional must satisfy to describe Mott-Hubbard behavior in the limit in which the one-band mapping is accurate is that the potential should have regions which scale as Z^0. Any functional whose xc potential scales to zero when $Z \to \infty$ (keeping U/t constant) cannot describe Mott-Hubbard behavior. As will be shown next, this is the case for all conventional functionals which, according to our definition, converge to an exchangelike contribution in the high-density limit.

D. Scaling properties

It is useful to recast our findings in terms of scaling relations, which are a basic tool for constructing approximate functionals in DFT (for a recent review, see, e.g., Ref. [46]). The density in atomic units reads as

$$\tilde{n}(\tilde{\mathbf{r}}) = \frac{Z^3}{a_B^3} n(\mathbf{r}) = \frac{Z^3}{a_B^3} n(Z\tilde{\mathbf{r}}/a_B). \tag{10}$$

If a were kept fixed, then the $Z \to \infty$ limit would correspond to the noninteracting case, which, in DFT, it is exactly equivalent to a density in atomic units driven to the high-density limit [Fig. 4(a)]. If instead $\tilde{a}$ were kept fixed then, in scaled units, atoms run away from each other [Eq. (2)] and atomic orbitals become asymptotically exact with [47]

$$\begin{aligned} t &= \frac{2}{3} a e^{-a}, \\ U &= \frac{5}{8Z}, \end{aligned} \tag{11}$$

implying that

$$t/U \sim Z^2 e^{-Z\tilde{a}/a_B} \tilde{a}/a_B \ll 1,$$

which corresponds to the strong-coupling limit of the Hubbard model [Fig. 4(b)]. Instead, here we change a with Z in such a way that t/U is kept constant [Fig. 4(c)]. In scaled units atoms run away from each other [although slower than the trivial scaling of Eq. (2)], thus, Eqs. (11) are still valid. Therefore, the condition of keeping t/U fixed can be obtained more precisely by solving the following equation for a:

$$a e^{-a} = \frac{15}{16Z} \frac{t}{U}, \tag{12}$$

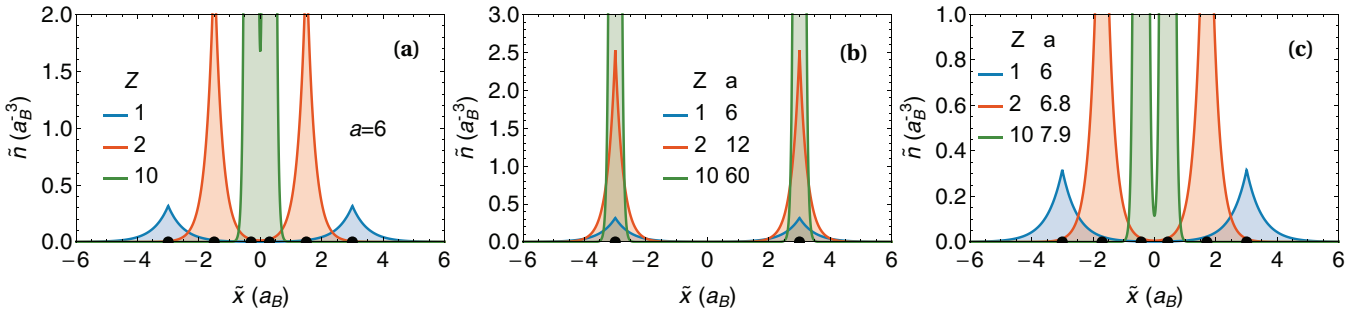

FIG. 4. Schematic plot of different scalings of the charge density in atomic units as a function of the position in units of the Bohr radius. The black dots indicate the position of the atoms. (a) The scaled distance is fixed at $a = 6$ ($a_B Z^{-1}$). As Z grows, the atoms approach each other in atomic units and the Hubbard interaction decreases as $U/t \sim 1/Z$. In scaled units, this panel will be qualitatively similar to Fig. 3. (b) The distance in atomic units is fixed at $\tilde{a} = 6a_B$ the scaled distance is shown in the legend. Here, $U/t \sim e^Z$ due to the exponential suppression of tunneling. (c) The scaled distance is fixed at $a = 6(a_B Z^{-1})$ for $Z = 1$ and then it is changed as $a \sim \ln Z$ so that $U/t \sim 70$ is kept constant (see legend). As Z grows, the atoms approach each other in atomic units and the density increases in the bond region, but both more slowly than in (a). Notice that in cases (a) and (c) the density in the bond is driven to the high-density limit where conventional functionals converge to the noninteracting limit despite $U/t \sim 70$ in case (b) corresponds to a highly stretched bond. Case (a) is the usual DFT scaling [46] to high density [Eq. (10)] and case (b) is the extreme stretched case, while case (c) is the scaling considered in this work.

which yields $a(Z) = -W_{-1}(-\frac{15t}{16ZU})$ with W the Lambert function. At large Z, the leading terms in $a(Z)$ are

$$a(Z \to \infty) = \ln(Z) + \ln[\ln(Z)] + \dots . \tag{13}$$

In atomic units, the atoms get closer to each other as Z grows [Fig. 4(c)]:

$$\tilde{a} \sim \frac{\ln Z}{Z} a_B.$$

We can now obtain the scaling of the density in the one-band constant U/t limit. It is easy to see that close to the atoms (i.e., at a fixed scaled distance $\mathbf{r}$ from the nuclei) the density in atomic units is given by the usual uniform scaling relation [Eq. (10)].

Solving the two-site problem with atomic orbitals we obtain that the correlated density at the mid-bond region in scaled units [Eq. (A11)] goes to zero as

$$n(0) = (1+q)\frac{2}{\pi} e^{-a} \sim \frac{1}{Z \ln(Z)}. \tag{14}$$

However, to analyze the DFT behavior we need the density in atomic units which behaves as

$$\tilde{n}(0) \sim Z^3 e^{-a(Z)} = \frac{Z^2}{\ln(Z)}, \tag{15}$$

which is still high density for large Z as illustrated in Fig. 4(c), but not in the usual uniform scaling way [Eq. (10)]. To the best of our knowledge, this scaling has not been considered before. Without the $\ln(Z)$ in the denominator, the scaling has been considered in Sec. IV E of Ref. [46], where, however, it has been analyzed only for low densities (which would correspond to $Z \to 0$ in our case).

Since, by definition, at high density conventional functionals converge to an exchangelike contribution, it follows they can not yield the parts of the potential scaling as Z^0. The dilemma of DFT is to keep these anomalous scaling parts of the potential in the high-density limit where conventional functionals converge to pure exchange. For details on specific functionals, see Appendix B.

IV. MOTT BARRIERS

How does the exact xc potential look? It should have a barrier in the bond to deplete the KS density, a well-known result from the study of molecules [48–53]. We term the part of the xc potential that scales as Z^0 a "Mott barrier." It can be proved that the barrier height in the strongly correlated regime is related to the ionization potential of the system [49–53]; it is therefore of order $O(Z^0)$ as expected from the previous arguments.

To illustrate the Mott-barrier effect and develop an approximation for the exact potential, we follow a long tradition [11,54] and study a two-site system as a proxy for the lattice. As in the pioneering works of Refs. [48–53] we compute the Hxc potential $v_{\rm Hxc} \equiv v_{\rm H} + v_{\rm xc}$, by inverting Kohn-Sham equations with the full CI densities as an input (Appendix H).

In Figures 5(a) and 5(b), we show the potential along the bond for $Z = 5$ and different interatomic distances. The dots and solid lines in Fig. 5(a) are obtained, respectively, by inverting CI densities and by approximate analytical formulas which will be explained later while the lines in Fig. 5(b) represent the LDA. We see that for large a (strong correlation), a large barrier develops in the bond while this effect is missed by the LDA. Notice that for the shortest distance a broad small barrier appears in the numerical results which is approximately reproduced in the LDA. This barrier is of a different physical origin and will be discussed below. Analogous conclusions can be drawn by looking at Figs. 5(c) and 5(d) where we plot the potential at fixed interatomic distance $a = 4.5$ ($a_B Z^{-1}$) for different values of Z. As shown by the squares in Fig. 2(b) by changing Z at this distance, one goes from the case of weak correlation ($Z = 5$, large q) to the case of strong correlation ($Z = 1$, small q). Indeed, a large barrier develops in the CI results for the last case which is not reproduced by the LDA which instead works well at weak coupling.

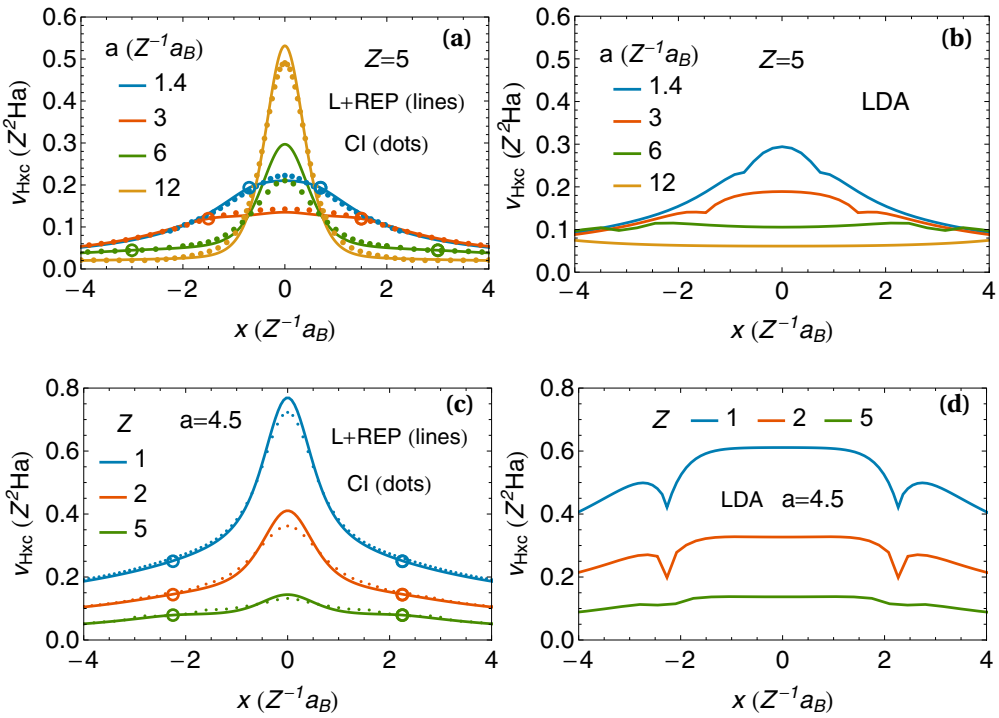

FIG. 5. Hartree-exchange-correlation potential for a two-site system. The potential is plotted along the bond direction x for $z = y = 0$ and different values of a and Z. Panels (a) and (c) show the potential obtained inverting the full CI density (dots) and in the L+REP approximation using orthogonalized atomic orbitals (lines). Open circles indicate the positions of the ions. Panels (b) and (d) show the LDA [43] results corresponding to panels (a) and (c). The strength of the correlations for each case is defined by the value of q in Fig. 2(b).

Figure 6 shows that the arguments developed rigorously for large Z still describe the behavior for $Z = 1$ changing a. Notice, however, that the barrier becomes smaller as one goes to larger a which may seem surprising according to our previous arguments. We will see below that the barrier has actually two components one with the Hartree-type $1/Z$ scaling and the other scaling, as expected from the previous arguments, as Z^0. It is the latter component which becomes large in the strong-coupling regime and which can not be captured by conventional functionals. Indeed, in all weak-coupling cases LDA approximately reproduces the barrier (apart from a constant shift which is only relevant in determining the tails of the density far from the molecule). In contrast, as correlations increase LDA starts to perform very badly.

The solid lines in Figs. 5(a), 5(c), and 6(a) represent a reverse-engineering potential (REP) obtained from an approximate analytical inversion of KS equations combined with the solution of the lattice problem (L+REP) constructed from orthogonalized $1s$ atomic orbitals (Appendixes D and E). This inversion, involving a Laplacian, is a singular problem so that subtle errors in the density propagate to give large errors in the potential and the task may seem hopeless with such a rough basis. Since a large source of error comes from the basis, we

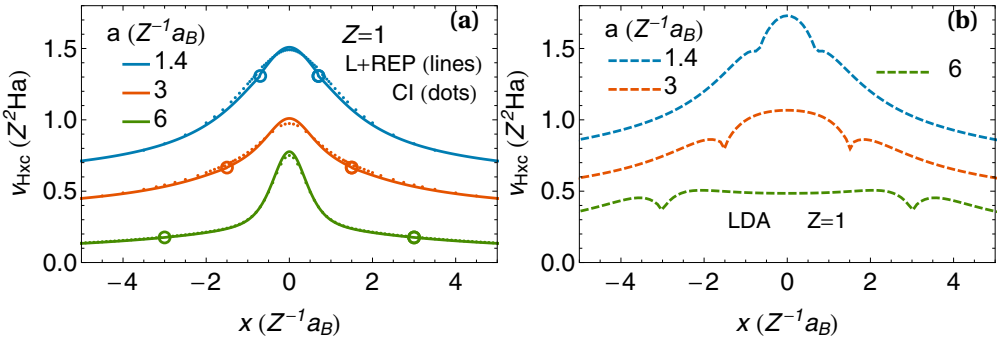

FIG. 6. Hartree-exchange-correlation potential for the stretched hydrogen molecule. We show v_{Hxc} as a function of x for $z = y = 0$ for different values of R. The dots in (a) were obtained inverting the full CI ground-state density as explained in Appendix H while the lines are the L+REP results. Open circles indicate the position of the ions. Panel (b) shows the LDA results. The cases $a = 1.4$ and $3(a_B Z^{-1})$ were shifted by 0.5 and 0.25 (Z^2 Ha), respectively, for clarity. The first two cases are in the weak and intermediate correlation regimes while the case $a = 6(a_B Z^{-1})$ is in the strong-coupling regime [cf. Figs. 2(b) and 7(b)].

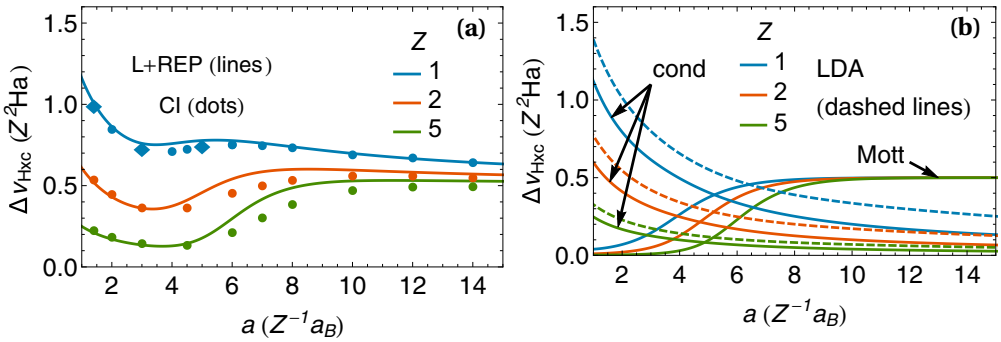

FIG. 7. Height of the Hartree exchange-correlation potential at the bond midpoint for the two-site system as a function of internuclear separation for different Z. In (a) full lines are obtained using the L+REP approximation subtracting a small spurious term at infinity [Eqs. (D21) and (D22)]. Dots are obtained inverting the full CI charges. For $Z = 1$, we include also data obtained with an accurate variational wave function (Appendix H). Diamonds are from Ref. [55]. (b) Shows separately the anomalously scaling Mott barrier height contribution, Eq. (D21), and the contribution scaling as $1/(Za)$ (cond) from Eq. (D22). The dashed lines are the LDA results.

first derive equations to optimize it (Appendix C and Refs. [38,39]). Fortunately, the solution of these equations is not needed. Instead, one finds that they can be used to eliminate the Laplacian, yielding equations which are much less sensitive to the basis and can be evaluated with approximate orbitals (Appendix F).

The resulting expressions for the Hartree-exchange-correlation potential read as

$$v_{\rm Hxc}(\mathbf{r}) = v_{\rm c}^{\rm kin}(\mathbf{r}) + v_{\rm xc}^{\rm resp}(\mathbf{r}) + v_{\rm Hxc}^{\rm cond}(\mathbf{r}), \tag{16}$$

with

$$v_{\rm c}^{\rm kin}(\mathbf{r}) = \frac{(1-q^2)}{2}\frac{|\phi_a(\mathbf{r})\vec{\nabla}\phi_b(\mathbf{r}) - \phi_b(\mathbf{r})\vec{\nabla}\phi_a(\mathbf{r})|^2}{n^2(\mathbf{r})}, \tag{17}$$

$$v_{\rm xc}^{\rm resp}(\mathbf{r}) = \frac{t(1-q)[\phi_a(\mathbf{r}) - \phi_b(\mathbf{r})]^2}{n(\mathbf{r})} + \delta\epsilon_g, \tag{18}$$

$$v_{\rm Hxc}^{\rm cond}(\mathbf{r}) = \frac{1}{Z}\int \frac{n_2(\mathbf{r},\mathbf{r}')}{n(\mathbf{r})|\mathbf{r}-\mathbf{r}'|}d\mathbf{r}', \tag{19}$$

where $\delta\epsilon_g > 0$ is a small positive constant and $n_2(\mathbf{r},\mathbf{r}')$ is the two-body density [55]. The terms correspond one by one to the partition of the xc potential obtained by Buijse *et al.* [55]. The present expressions, however, in terms of the lattice hopping reduction factor q are new.

As shown in Figs. 5 and 6, using L+REP Eqs. (17)–(19) yield a very accurate xc potential from the weakly to the strongly correlated regime. This holds even in the case $Z = 1$ where the influence of higher-energy orbitals could have spoiled the agreement.

The first term in Eq. (16) is order Z^0 while the last two terms are at most of order $1/Z$, thus, these equations show explicitly that the $v_{\rm xc}$ has parts with anomalous coupling constant scaling. Specifically, the first term, which vanishes in the weakly correlated limit ($q = 1$), yields the Mott barrier. The nonconstant part of Eq. (18) is of order $1/Z$ because of the t factor and our requirement of constant U/t.

In the one-band (large-Z) limit and for large a the above equations become particularly simple for the barrier height. Subtracting a small spurious constant term, there is no contribution from $v_{\rm xc}^{\rm resp}$ and the height separates in two contributions, one of Mott-Hubbard type, scaling as Z^0, and one of Coulomb form with different Z scaling,

$$v_{\rm c}^{\rm kin}(0) \simeq \frac{(1-q)}{2(1+q)}, \tag{20}$$

$$v_{\rm Hxc}^{\rm cond}(0) \simeq \frac{1}{Za}. \tag{21}$$

Figure 7(a) shows the barrier height as a function of a for different Z. The dots are the numerical data, while the full lines are obtained from Eqs. (D21) and (D22). Figure 7(b) shows the barrier separated in the two components. LDA yields a quite good account of the Z^{-1} component while the Z^0 component is completely missed. One can also see that the Z^0 component just reflects the q behavior as a function of distance shown in Fig. 2.

For hydrogen [upper curve in Fig. 7(a)], an accidental compensation of the distance dependence of the two components explains why the crossover was not identified in the potential before.

V. GENERALIZATION TO MANY ATOMS

To illustrate the relevance of these results for extended systems, we introduce a simple generalization of the L+REP equations (17)–(19) to the many-atom many-electron case. Equation (19) can be used without modification. Equations (17) and (18) are important only in the strong correlation regime. In this case, since electrons are localized, we expect that the wave function resembles the two-site wave function. Thus, Eqs. (17) and (18) are generalized by replacing the site labels a and b by site indexes i and j and summing over all $\langle i,j\rangle$ nearest-neighbor sites. q is obtained from the solution of the lattice problem in the geometry considered (see Appendix G).

Figure 8(a) shows the barriers for a four-site H chain while Fig. 8(b) compares a quantum chemistry computation of the charge with the KS charge corresponding to the L+REP potential. The small difference between the two charges indicates that the L+REP is accurate also in this case.

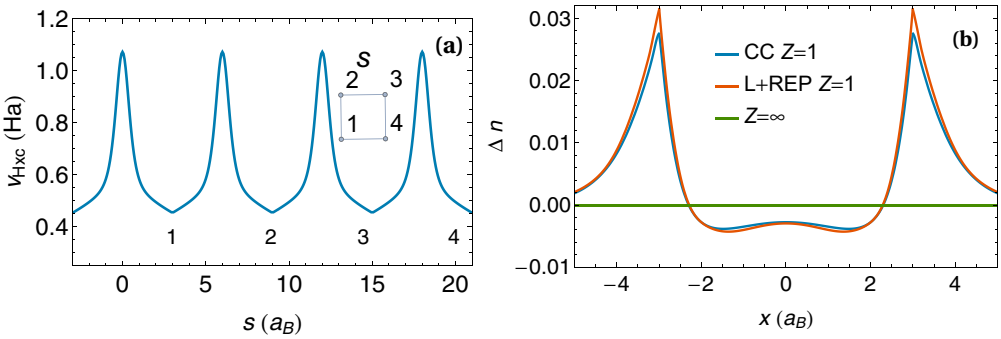

FIG. 8. Mott barriers for a four-atom chain. Panel (a) shows v_{Hxc} along the path shown in the inset for four H atoms arranged in a square with interatomic distance $a = 6a_B$. Panel (b) compares the interacting charge computed with an accurate quantum chemistry method (CC) and the charge from the solution of the Kohn-Sham potential obtained with the L+REP method. Both are displayed as the difference between the interacting and the noninteracting charge ($Z = \infty$) along one side of the square with the origin at the bond midpoint.

VI. DISCUSSION AND CONCLUSION

We have studied a model which shows Mott-Hubbard phenomena in a limit in which DFT and a lattice approach are forced to agree quantitatively. In this one-band limit with constant U/t, a dichotomy appears between two paradigmatic descriptions of interacting electrons, namely, the one-band Hubbard model and Kohn-Sham DFT. No matter how large is Z, the exact Kohn-Sham orbitals cannot be expanded in terms of the $1s$ band alone and, for a successful description of Hubbard-type correlations within Kohn-Sham DFT, one is obliged to consider other orbitals, in contrast to the one-band Hubbard description where the density is computed without information on the higher bands.

A basic aspect of Mott-Hubbard physics is the suppression of the tunneling amplitude in the lattice model which is equivalent to a suppression of bond charge in the continuum model. The way in which exact Kohn-Sham DFT manages to reproduce the correlated density is by the appearance of Mott barriers in the bonds which mix the Kohn-Sham orbitals of the band of interest with other bands.

Basically, we have shown that in the one-band limit keeping U/t constant the exchange-correlation potential has parts which remain finite despite the fact that the coupling constant is formally driven to zero. Conventional functionals can not cope with this situation and, therefore, they are generically inadequate to describe Mott phenomena or stretched bonds. This is the case of widely used functionals such as local, semilocal, strictly correlated electrons and hybrids among others.

Van Leeuwen and Baerends [56] had carefully analyzed the behavior of a generalized gradient approximation (GGA) exchange-correlation potential, namely, the so-called B88 exchange [3] with P86 correlation [57]. Their conclusion is that for hydrogen molecule, these functionals yield a barrier in the midpoint region that is divergent in the dissociation limit instead of having a constant height, thus, the barrier appears "too large." As shown in Appendix B in the one-band limit the barrier vanishes, thus, it is shown to be "too small." This appears paradoxical as both results correspond to the limit of infinite atomic separation. However, in Ref. [56] the Hubbard-type interaction strength as measured by U/t also diverges while in our computation it is kept constant. In that sense, those functionals yield barriers which are too small to describe Mott-Hubbard behavior although they may mimic real Mott barriers for specific values of coupling constant and distance. This may explain why these functionals appear to work on some materials and molecules but not in others. Clearly, they lack the generality needed for being predictive in all situations although they may improve over LDA in specific situations.

The bond-charge problem studied here provides different insight with respect to the fractional charge and fractional spin analysis [58], which corresponds to the very stretched limit. Here, we analyze explicitly a less extreme case, gaining important information on the more challenging intermediate correlation regime.

It is often assumed that Kohn-Sham DFT bands do not show any narrowing due to interactions. Our results clearly indicate that the exact Kohn-Sham DFT bands will show band narrowing due to a suppression of tunneling stemming from Mott barriers [cf. Figs. 5(a), 5(c), 6(b), and 8(a)]. However, we have also shown that as soon as any conventional local semilocal or hybrid functional is used, this effect is lost. Thus, although the assumption is in principle incorrect, in most practical computations available at present it is correct because the Mott barrier effect is not included.

We find that the xc potential separates naturally into two components, one with a conventional coupling constant scaling $(1/Z)$ and one with an anomalous coupling constant scaling Z^0. Standard functionals capture only the first component, thus, those approaches in which Mott-Hubbard correlations are incorporated at a second stage modifying the conventional DFT band structure through DMFT or Gutzwiller approximations can be seen as a way to take into account the missing component [20,26–29]. Our results establish a firm theoretical basis to reformulate this approach in a rigorous way, avoiding double-counting problems which plague the field. Indeed, there is a clear division of the work that needs to be done by each approach related to the scaling properties of the potential.

Clearly, to obtain the anomalous coupling constant scaling directly from a functional is a highly nontrivial task. The present L+REP approach is a shortcut to this problem. In particular, Eq. (17) establishes an intimate relationship between the suppression of tunneling in the lattice model and

in the Kohn-Sham description linking in a neat way the two worlds of lattice models and DFT in the continuum.

ACKNOWLEDGMENTS

This work was supported by the Italian Institute of Technology through the project NEWDFESCM and Italian MIUR under project PRIN-RIDEIRON-2012X3YFZ2. V.B. acknowledges financial support by Italian MIUR under project FIRB-HybridNanoDev-RBFR1236VV and Premiali-2012 AB-NANOTECH. P.G.-G. acknowledges financial support from the European Research Council under H2020/ERC Consolidator Grant corr-DFT (Grant No. 648932). Z.-J.Y acknowledges financial support from the Future and Emerging Technologies (FET) program under FET-Open Grant No. 618083 (CNTQC). D.V. acknowledges partial support from the EU Centre of Excellence "MaX-Materials Design at the Exascale" (Grant No. 676598).

APPENDIX A: LATTICE MODEL AND GUTZWILLER WAVE FUNCTION

The one-band model is obtained by expanding the field operators $\psi_\sigma(\mathbf{r})$ and $\psi^\dagger_\sigma(\mathbf{r})$ in a minimal basis consisting of N Wannier orbitals $\phi_i(\mathbf{r}) \equiv \langle \mathbf{r}|i\rangle$ centered on the N sites of the lattice

$$\psi_\sigma(\mathbf{r}) = \sum_{i\sigma} \phi_i(\mathbf{r}) c_{i\sigma} + \ldots,$$
$$\psi^\dagger_\sigma(\mathbf{r}) = \sum_{i\sigma} \phi^*_i(\mathbf{r}) c^\dagger_{i\sigma} + \ldots, \tag{A1}$$

where the ellipsis indicates neglected higher-energy states. For the scaling arguments it is enough to define $\phi_i(\mathbf{r})$ as Wannier orbitals obtained from the lower band of Bloch states that diagonalize the noninteracting Hamiltonian (noninteracting Wannier orbitals). In the one-band limit defined in the text, they are very similar to orthogonalized atomic $1s$ orbitals. More accurate Wannier orbitals are discussed below.

Using Eqs. (A1), the one-band generalized Hubbard Hamiltonian corresponding to the continuum model defined in Eq. (3) can be cast as

$$H_{1\mathrm{B}} = H_h + H_w = \sum_{ij\sigma} h_{ij} c^\dagger_{i\sigma} c_{j\sigma} + \frac{1}{2} \sum_{ijkl\sigma\sigma'} w_{ij,kl} c^\dagger_{k\sigma} c^\dagger_{i\sigma'} c_{j\sigma'} c_{l\sigma} \tag{A2}$$

with $h_{ij} = \langle i|\hat{h}|j\rangle$ and

$$w_{ij,kl} = \int d^3\mathbf{r}\, d^3\mathbf{r}' \phi^*_k(\mathbf{r}) \phi^*_i(\mathbf{r}') w(\mathbf{r},\mathbf{r}') \phi_j(\mathbf{r}') \phi_l(\mathbf{r}), \tag{A3}$$

with $w(\mathbf{r},\mathbf{r}')$ denoting Coulomb interaction:

$$w(\mathbf{r},\mathbf{r}') = \frac{1}{Z|\mathbf{r}-\mathbf{r}'|}. \tag{A4}$$

$H_{1\mathrm{B}}$ is written in terms of bare matrix elements as, for example, the onsite Coulomb interaction $U_0 \equiv w_{ii,ii}$. The effect of orbitals outside the basis is often accounted for [20] by replacing the bare matrix elements by screened matrix elements. However, in the one-band limit this effect can be neglected (see Fig. 1) and we drop the nought (i.e., $U_0 = U$).

Equations (A1) can be also employed to relate the one- and two-particle densities, respectively, $n(\mathbf{r})$ and $n_2(\mathbf{r},\mathbf{r}')$ to the one- and two-particle lattice density matrices as follows:

$$n(\mathbf{r}) = \sum_\sigma \langle \psi^\dagger_\sigma(\mathbf{r}) \psi_\sigma(\mathbf{r})\rangle = \sum_{ij} \phi^*_j(\mathbf{r}) \phi_i(\mathbf{r}) \rho_{ij} \tag{A5}$$

and

$$n_2(\mathbf{r},\mathbf{r}') = \sum_{\sigma\sigma'} \langle \psi^\dagger_{\sigma'}(\mathbf{r}') \psi^\dagger_\sigma(\mathbf{r}) \psi_\sigma(\mathbf{r}) \psi_{\sigma'}(\mathbf{r}')\rangle = \sum_{ijkl} \phi^*_i(\mathbf{r}) \phi_j(\mathbf{r}) \phi^*_k(\mathbf{r}') \phi_l(\mathbf{r}') D_{ij,kl}, \tag{A6}$$

where we defined the spin-integrated two-body lattice density matrix $D_{ij,kl} = \sum_{\sigma\sigma'} \langle c^\dagger_{i\sigma} c^\dagger_{k\sigma'} c_{l\sigma'} c_{j\sigma}\rangle$. The density of the Hartree state is recovered by inserting in Eq. (A5) the Hartree lattice density matrix ρ^H_{ij}, i.e., for two sites $\rho^H_{ab} = 1$, while for a chain of atoms,

$$\rho^H_{ab} = \frac{2}{N} \sum_{|ka|<\pi/2} \cos ka = \frac{2}{\pi}. \tag{A7}$$

Let us now focus on the two-site case. Labeling the two sites as a,b and assuming real orbitals, the one-particle lattice Hamiltonian is simply defined by $v = h_{aa} = h_{bb}$ and $-t = h_{ab}$, while the Coulomb operator reads as [21,37]

$$H_w = U \sum_{i=a,b} n_{i\uparrow} n_{i\downarrow} + V n_a n_b + t_c \sum_\sigma (n_{a\bar{\sigma}} + n_{b\bar{\sigma}})(c^\dagger_{a\sigma} c_{b\sigma} + \mathrm{H.c.}) + K \sum_{\sigma\sigma'} c^\dagger_{a\sigma} c^\dagger_{b\sigma'} c_{a\sigma'} c_{b\sigma} + K' \sum_\sigma c^\dagger_{a\sigma} c^\dagger_{a\bar{\sigma}} c_{b\bar{\sigma}} c_{b\sigma}, \tag{A8}$$

where $V = w_{aa,bb}$ denote the intersite repulsion, $K = w_{ab,ba}$ is the direct exchange interaction, $K' = w_{ab,ab}$ can be thought as a Coulomb repulsion among bond charges, alternatively it can be seen as a pair-hopping term. For real orbitals, $K = K'$. Eventually, $t_c = w_{aa,ab}$ is a correlated hopping term and it can be considered as the contribution of the Hartree potential to the hopping.

The two-site lattice model can be solved exactly. The ground-state energy is given by

$$E_G = \tfrac{1}{2}(U + V + K + K' - \Delta^{Gw}),$$

where

$$\Delta^{Gw} = \sqrt{(U - V - K + K')^2 + 16(t - t_c)^2}.$$

The ground state is

$$|\Psi_{s,0}\rangle = \frac{|\Phi_{\mathrm{HL}}\rangle + \gamma |\Phi_{\mathrm{ion}}\rangle}{\sqrt{1+\gamma^2}}, \tag{A9}$$

where $|\Phi_{\rm HL}\rangle$ and $|\Phi_{\rm ion}\rangle$ are defined by

$$|\Phi_{\rm HL}\rangle = \frac{1}{\sqrt{2}}(c^\dagger_{a\uparrow}c^\dagger_{b\downarrow} + c^\dagger_{b\uparrow}c^\dagger_{a\downarrow})|\emptyset\rangle,$$

$$|\Phi_{\rm ion}\rangle = \frac{1}{\sqrt{2}}(c^\dagger_{a\uparrow}c^\dagger_{a\downarrow} + c^\dagger_{b\uparrow}c^\dagger_{b\downarrow})|\emptyset\rangle$$

and γ is given by

$$\gamma = \frac{\Delta^{Gw} - (U - V - K + K')}{4(t - t_c)}. \tag{A10}$$

The correlated density Eq. (A5) reads as

$$n(\mathbf{r}) = \phi_a^2(\mathbf{r}) + \phi_b^2(\mathbf{r}) + 2q\phi_a(\mathbf{r})\phi_b(\mathbf{r}) \tag{A11}$$

with the hopping reduction factor

$$q = \frac{2\gamma}{1+\gamma^2}. \tag{A12}$$

Figure 2(b) was obtained from Eqs. (A3), (A10), and (A12) using orthogonalized atomic $1s$ orbitals (Appendix E).

1. Gutzwiller wave function

The correlation-induced changes in bond charges described by q are rooted in the competition between tunneling energy and Coulomb induced localization. For extended systems, the Gutzwiller wave function is a simple tool to study such competition.

For a lattice of identical atoms, the Gutzwiller wave function can be written as [22,40,59]

$$|\Psi_\gamma\rangle = \frac{\gamma^D}{C_\gamma^{1/2}}|\Psi_0\rangle, \tag{A13}$$

where $|\Psi_0\rangle$ is a Slater determinant, $D = \sum_i n_{i\uparrow}n_{i\downarrow}$ counts the total double occupancy, γ is a variational parameter, and $C_\gamma = \langle\Psi_0|\gamma^{2D}|\Psi_0\rangle$ a normalization constant. For $U > 0$, the operator γ^D decreases the weight of configurations with double occupied sites. The Gutzwiller variational problem can be solved exactly in infinity and in one dimension [33,34].

In the two-site case, the Gutzwiller wave function coincides with the exact expression given in Eq. (A9), and interpolates between the Hartree-Fock (HF) and the Heitler-London (HL) solutions recovered, respectively, for $\gamma = 1$ and 0.

Unlike the two-atom case, the Gutzwiller wave function does not yield the exact solution of the infinite-dimensional problem. However, comparing with the exact solution which can be obtained numerically using dynamical mean-field theory, one finds that it gives a remarkably accurate description of the metallic phase [see Fig. 2(a)]. In the insulating phase it yields $q = 0$, in contrast with the finite value of q of the exact solution. Furthermore, the exact solution shows a Mott transition at the kink position in the blue curve of Fig. 2(a), while in the Gutzwiller approximation the transition occurs at $U = U_{\rm BR}$ with $U_{\rm BR}$ denoting the Brinkman-Rice U [32].

APPENDIX B: TESTING FUNCTIONALS

The dimensionless Hamiltonian of Eq. (3) reads as

$$\hat{H}(Z,a) = \hat{T} + \hat{V}_{\rm ext}(a) + \frac{1}{Z}\hat{V}_{ee}, \tag{B1}$$

where

$$\hat{T} = -\sum_i^N \frac{1}{2}\nabla^2_{\mathbf{r}_i} \tag{B2}$$

$$\hat{V}_{\rm ext}(a) = -\sum_{ij}^N \frac{1}{|\mathbf{r}_i - \mathbf{R}_j|}, \tag{B3}$$

$$\hat{V}_{ee} = \frac{1}{2}\sum_{ij}^N \frac{1}{|\mathbf{r}_i - \mathbf{r}_j|}, \tag{B4}$$

and we made explicit the a dependence of the external potential.

We now analyze the consequence of the high-density scaling of Eq. (15) in the exchange-correlation functional. Consider the Hohenberg-Kohn functional for the Hamiltonian (B1):

$$F_Z[n] = \min_{\Psi\to n}\langle\Psi|\hat{T} + \frac{1}{Z}\hat{V}_{ee}|\Psi\rangle, \tag{B5}$$

where the minimization is over all wave functions yielding the given density. The Kohn-Sham potential is given by the functional derivative

$$v_{\rm Hxc}(\mathbf{r}) = \frac{\delta T_c[n,Z]}{\delta n(\mathbf{r})} + \frac{1}{Z}\frac{\delta V_{ee}[n,Z]}{\delta n(\mathbf{r})}, \tag{B6}$$

where $T_c[n,Z]$ is the difference between the exact kinetic energy $\langle\Psi[n,Z]|\hat{T}|\Psi[n,Z]\rangle$ and the KS one, and $V_{ee}[n,Z] = \langle\Psi[n,Z]|\hat{V}_{ee}|\Psi[n,Z]\rangle$, with $\Psi[n,z]$ the minimizing wave function in Eq. (B5).

It can be shown [50] that the two functionals in Eq. (B5) can be written as

$$T_c[n] = \int n(\mathbf{r})v_c^{\rm kin}([n],\mathbf{r})d\mathbf{r}, \tag{B7}$$

$$\frac{1}{Z}V_{ee}[n] = \frac{1}{2}\int n(\mathbf{r})v_{\rm Hxc}^{\rm cond}([n],\mathbf{r})d\mathbf{r}, \tag{B8}$$

where $v_{\rm Hxc}^{\rm cond}$ and $v_c^{\rm kin}$ can be defined in terms of correlated density matrices. Performing the functional derivative (B6), one obtains

$$\frac{\delta T_c[n]}{\delta n(\mathbf{r})} = v_c^{\rm kin}([n],\mathbf{r}) + \int n(\mathbf{r}')\frac{\delta v_c^{\rm kin}([n],\mathbf{r}')}{\delta n(\mathbf{r})}d\mathbf{r}', \tag{B9}$$

$$\frac{1}{Z}\frac{\delta V_{ee}[n]}{\delta n(\mathbf{r})} = v_{\rm Hxc}^{\rm cond}([n],\mathbf{r}) + \int n(\mathbf{r}')\frac{\delta v_{xc}^{\rm cond}([n],\mathbf{r}')}{\delta n(\mathbf{r})}d\mathbf{r}'. \tag{B10}$$

This is the same partition of Eq. (16) with the potentials expressed in terms of correlation functions but which, as mentioned above, at the equilibrium density coincide one by one with our expressions with $v_{\rm xc}^{\rm resp}$ given by the sum of the second terms in Eqs. (B9) and (B10). In particular, we recover the known result that the barrier is due to the correlation kinetic energy part of the exchange-correlation functional [53,55] and which here is identified with the anomalous scaling part of the potential.

Normally (keeping a fixed), in the limit $Z \to \infty$ the physical kinetic energy functional tends to the KS kinetic functional, so that $T_c[n,Z] \to 0$, together with its functional derivative, and there is no part of the potential that scales

like Z^0. Here, instead, imposing Eq. (13) (fixing t/U), we find that the first term in the functional derivative of $T_c[n,Z]$ [Eq. (B9)] stays finite. In the same region where $v_c^{\rm kin}(\mathbf{r})$ stays finite, the scaled density is vanishing [Eq. (14)] so that $T_c[n,Z]$ for $Z\to\infty$ goes to zero, but not its functional derivative.

1. Functionals based on the expectation of V_{ee}

Any approximate functional that uses the expectation value of $\hat{V}_{ee}$ on some wave function is doomed to fail for the Mott barrier, as it will inherit the $1/Z$ prefactor in front of $\hat{V}_{ee}$, as shown by Eq. (B6). Simply, neglecting the T_c part of the Kohn-Sham functional, can not be compensated by the interaction part. This is the case of the strictly correlated electron functional, which corresponds to the minimum possible expectation value of $\hat{V}_{ee}$ in a given density. Its functional derivative is finite everywhere [60] and it is not going to compensate the $1/Z$ factor (see also Fig. 6 of Ref. [61]). Hybrid functionals, which use the expectation value of $\hat{V}_{ee}$ on the Hartree-Fock (HF) wave function, have the same problem for their nonlocal exchange part (in a restricted formalism, of course, which is the focus of this paper). For example, in the simple case $N=2$, both HF and exact exchange reduce to minus $\frac{1}{2}$ the Hartree potential, a perfectly smooth function that is not going to blow up to compensate the $1/Z$ prefactor.

Hybrid functionals have also a generalized gradient approximation (GGA) component which is analyzed below.

2. Local and semilocal functionals

Local and semilocal functionals directly model $T_c[n]$ together with the xc part of V_{ee}. The xc potential of LDA and GGA functionals can be written in terms of atomic units and scaled units as

$$\begin{aligned} v_{\rm xc} &= v_{\rm xc}\big(a_B^3\tilde{n}, a_B^4\tilde{\nabla}\tilde{n}, a_B^5\tilde{\nabla}^2\tilde{n},\dots\big) \\ &= v_{\rm xc}(Z^3 n, Z^4\nabla n, Z^5\nabla^2 n,\dots). \end{aligned} \tag{B11}$$

It is convenient to interrogate functionals at the midpoint of an homoatomic bond where the part of the potential scaling as Z^0 should be larger, and the density scales as in Eq. (15).

We are interested in the high-density limit of functionals (Sec. III D). For the LDA, gradient terms are not present and $v_{\rm xc}$ behaves as [62]

$$\begin{aligned} v_{\rm xc}^{\rm LDA} &= A a_B \tilde{n}^{1/3}\ \text{Ha} \\ &= A\frac{1}{Z} n^{1/3} \sim \frac{1}{Z^{4/3}[\ln(Z)]^{1/3}} \quad (Z^2\ \text{Ha}), \end{aligned} \tag{B12}$$

where A is a constant and the second line shows that in rescaled units $v_{\rm xc}^{\rm LDA}(0)\to 0$. Imposing self-consistency does not change this result since the density is driven to the noninteracting density which is given by Eq. (14) with $q=1$. One can also consider points which are at a fixed position with respect to the nucleus in rescaled units. In this case, the rescaled density remains asymptotically constant as Z grows and $v_{\rm Hxc}^{\rm LDA}\sim 1/Z$. Therefore, since there is not term scaling as Z^0, we conclude that LDA can not describe Mott phenomena in the one-band limit.

For other functionals, specific forms must be considered as the final result will depend on the scaling properties of the potential. However, in general the behavior will be dominated by the high-density limit of the functional where, by construction, conventional functionals converge to the noninteracting limit and, therefore, have no portions scaling as Z^0 in rescaled units.

As an explicit example, we follow Van Leeuwen and Baerends [56] and we evaluate the potential at the origin with the GGA corresponding to Becke (B88) exchange [3,63] and Perdew's correlation (P86) [57]. It was found that both contributions have the same functional form at the midpoint but with a different multiplicative constant so that the sum can be written as

$$\begin{aligned} v_{\rm xc}^{\rm GGA} &= B a_B \frac{\nabla^2\tilde{n}}{\tilde{n}^{4/3}}\text{Ha} = B\frac{1}{Z}\frac{\nabla^2 n}{n^{4/3}} = B\frac{1}{Z}\frac{1}{n(0)^{1/3}} \\ &\sim B\frac{(\ln Z)^{1/3}}{Z^{2/3}} \quad (Z^2\text{Ha}) \end{aligned} \tag{B13}$$

with $B>0$. By letting $Z\to\infty$, one sees that the potential goes to zero more slowly than LDA but still not enough to provide the barrier. Again, self-consistency does not improve the result.

Meta-GGA functionals, which use the KS kinetic energy density as input ingredient, are normally used in the generalized KS framework, leading to single-particle equations with a different structure than (D1) (e.g., with the gradient of the orbitals). For this reason, the analysis of the barrier carried out here is not directly applicable in this context. We remark that meta-GGA's also lead to symmetry breaking for stretched bonds, with the problems listed in the Introduction.

APPENDIX C: OPTIMUM BASIS SET

As mentioned in main text and noted by several authors (see, e.g., [64]), the inversion of KS equations to determine the KS potential is a difficult task. For example, the value of the KS potential with respect to the value at infinity (assumed to be zero) is determined by the decay rate of the tail of the density far away from the nuclei [65]. Therefore, an exponentially small error in the density coming from an approximate orbital basis can produce an order-one error in the potential. Thus, we first present a computation of the optimum minimal basis set to expand the field operator. For simplicity, we restrict to a lattice wave function which depends on the single parameter γ, but the method can be easily generalized to the full set of parameters which specify the lattice wave function [39].

The variational energy is written as a functional of the Wannier states to be optimized and of the parameters that specify the lattice wave function as follows [38,39]:

$$\begin{aligned} E[\phi_i,\phi_i^*,\gamma] = &\sum_{ij} h_{ij}\rho_{ji} + \frac{1}{2}\sum_{ijkl} w_{ij,kl} D_{kl,ij} \\ &+ \sum_{ij}\Omega_{ij}(\langle\phi_i|\phi_j\rangle - \delta_{ij}), \end{aligned} \tag{C1}$$

where Ω_{ij} is a Hermitian matrix of Lagrange parameters that implements the constraint of the orthonormality of the orbitals.

The variation with respect to ϕ_i^* leads to

$$\sum_j \left(\rho_{ij} \hat{h}(\mathbf{r}) + \sum_{kl} D_{ij,kl} w_{kl}(\mathbf{r}) - \Omega_{ij} \right) \phi_j(\mathbf{r}) = 0, \quad \text{(C2)}$$

where we introduced the potential

$$w_{kl}(\mathbf{r}) = \int d\mathbf{r}' \phi_k^*(\mathbf{r}') w(\mathbf{r},\mathbf{r}') \phi_l(\mathbf{r}').$$

Along with the minimization with respect to γ, Eq. (C2) defines a set of closed integrodifferential equations. Both problems have to be solved self-consistently since the electronic matrix elements in Eq. (A10) depend on the orbitals [Eq. (A3)] which in turn depend on the lattice density matrices through Eq. (C2). The latter can be further simplified by transforming to the natural orbital basis [39] where the one-body density matrix and the Lagrange multiplier matrix become diagonal $\bar{\rho}_{\mu\nu} = \delta_{\mu\nu}\bar{\rho}_\mu$ with the bar denoting matrix elements in the rotated basis.

Now, we restrict to the two-site case. Minimization respect to γ yields back Eq. (A10). The natural orbitals are

$$\psi_0(\mathbf{r}) = \frac{\phi_a(\mathbf{r}) + \phi_b(\mathbf{r})}{\sqrt{2}}, \quad \psi_1(\mathbf{r}) = \frac{\phi_a(\mathbf{r}) - \phi_b(\mathbf{r})}{\sqrt{2}} \quad \text{(C3)}$$

and the density matrix takes the familiar Gutzwiller form [40,59]

$$\bar{\rho}_0 = 1 + q, \qquad \bar{\rho}_1 = 1 - q, \quad \text{(C4)}$$

with q given by Eq. (A12), while for D we have

$$\bar{D}_{00,00} = 1 + q, \quad \bar{D}_{11,11} = 1 - q,$$
$$\bar{D}_{10,10} = \bar{D}_{01,01} = -\sqrt{1 - q^2}, \quad \text{(C5)}$$

all other elements vanish. The equations for the states ψ_μ can be cast as effective single-particle equations, i.e.,

$$\left(-\tfrac{1}{2}\nabla^2 + v_{\text{ext}} + v_\mu(\mathbf{r})\right)\psi_\mu = \omega_\mu \psi_\mu, \quad \text{(C6)}$$

where we set $\Omega_\mu = \rho_\mu \omega_\mu$ and the potentials v_0 and v_1 are defined by

$$v_0(\mathbf{r}) = \bar{w}_{00}(\mathbf{r}) - \sqrt{\frac{1-q}{1+q}} \bar{w}_{01}(\mathbf{r}) \frac{\psi_1(\mathbf{r})}{\psi_0(\mathbf{r})}, \quad \text{(C7)}$$

$$v_1(\mathbf{r}) = \bar{w}_{11}(\mathbf{r}) - \sqrt{\frac{1+q}{1-q}} \bar{w}_{10}(\mathbf{r}) \frac{\psi_0(\mathbf{r})}{\psi_1(\mathbf{r})}. \quad \text{(C8)}$$

Eventually, one can solve equations (C6)–(C8) to obtain the natural orbitals and invert Eq. (C3) to obtain the Wannier orbitals [39]. In the following, we will not follow this route but we will use the above expressions to derive a set of equations for the xc potential that can be evaluated directly with approximate orbitals.

APPENDIX D: REVERSE-ENGINEERING POTENTIAL

Here, we derive the L+REP equations (17)–(19) for a homoatomic bond. For a closed-shell system, the Kohn-Sham equations read as

$$\left(-\tfrac{1}{2}\nabla^2 + v_{\text{KS}}(\mathbf{r}) - \epsilon_k\right)\varphi_k(\mathbf{r}) = 0, \quad \text{(D1)}$$

where v_{KS} is given by Eq. (9). The density is given by

$$n(\mathbf{r}) = 2 \sum_{k \in \text{occ}} \varphi_k^*(\mathbf{r}) \varphi_k(\mathbf{r}), \quad \text{(D2)}$$

where k labels the Kohn-Sham states and the sum runs over occupied states.

For two-electron systems only the $k = 0$ state is populated in Eq. (D2) so

$$\varphi_0(\mathbf{r}) = \sqrt{\frac{n(\mathbf{r})}{2}}$$

and the effective Kohn-Sham potential can be easily expressed as follows up to a constant ϵ_0:

$$v_{\text{KS}}(\mathbf{r}) = \epsilon_0 + \frac{\nabla^2 \sqrt{n(\mathbf{r})}}{2\sqrt{n(\mathbf{r})}}. \quad \text{(D3)}$$

The constant can be determined by requiring that the potential at infinity is zero which defines ϵ_0 as the highest occupied Kohn-Sham orbital eigenvalue. According to DFT Koopmans theorem [65,66], it is related to the ionization energy by $\epsilon_0 = -E_I$.

Subtracting the external potential one obtains the Hartree-exchange-correlation potential v_{Hxc} [cf. Eq. (9)]

$$v_{\text{Hxc}}(\mathbf{r}) = v_{\text{KS}}(\mathbf{r}) - v_{\text{ext}}(\mathbf{r}). \quad \text{(D4)}$$

Given two Wannier orbitals, ϕ_a and ϕ_b, to expand the lattice model (not necessarily optimized) we can define bonding and antibonding orbitals as in Eq. (C3). The density of the two-site problem (A11) can be rewritten in this basis set as

$$n(\mathbf{r}) = \sum_{\mu=0,1} \bar{\rho}_\mu \psi_\mu^2(\mathbf{r}) = (1+q)\psi_0^2(\mathbf{r}) + (1-q)\psi_1^2(\mathbf{r}). \quad \text{(D5)}$$

Replacing Eq. (D5) in Eqs. (D3) and (D4), the Hxc potential v_{Hxc} can be written as the sum of two contributions:

$$v_{\text{Hxc}} = v_{\text{c}}^{\text{kin}} + v_{\text{Hxc}}^{\text{rc}}, \quad \text{(D6)}$$

where

$$v_{\text{c}}^{\text{kin}} = \frac{(1-q^2)}{2} \frac{|\psi_1(\mathbf{r})\vec{\nabla}\psi_0(\mathbf{r}) - \psi_0(\mathbf{r})\vec{\nabla}\psi_1(\mathbf{r})|^2}{n^2(\mathbf{r})}, \quad \text{(D7)}$$

$$v_{\text{Hxc}}^{\text{rc}} = \frac{\sum_\mu \bar{\rho}_\mu \psi_\mu(\mathbf{r}) \nabla^2 \psi_\mu(\mathbf{r})}{2\, n(\mathbf{r})} - v_{\text{ext}}(\mathbf{r}) - E_I. \quad \text{(D8)}$$

Transforming back to atomic orbitals in the first equation, one obtains Eq. (17). Ironically, the contribution to v_{Hxc} which is the hardest to conventional DFT methods, i.e., the part scaling as Z^0, does not require further work and is already in its final form for numerical evaluation with suitable approximate orbitals (we use orthogonalized atomic orbitals as discussed in Appendix E). Furthermore, setting $q = 0$ one recovers the exact results of Helbig *et al.* [cf. Eq. (11) of Ref. [53]] in the extremely correlated case which are here generalized to arbitrary correlation.

We find, however, that evaluation of the remaining terms with approximate orbitals yields a potential in gross disagreement with numerical methods due to the presence of the Laplacian in Eq. (D8) (see Appendix F). Thus, in the following we assume that the orbitals are optimized. Surprisingly, this

condition can be relaxed in the final equations, effectively eliminating the strong sensitivity to the basis.

Inserting the optimization equations (C7) and (C8) in (D8), we can cancel the external potential term and eliminate the Laplacian to obtain

$$v_{\rm Hxc}^{\rm rc}(\mathbf{r}) = -\frac{\sum_\mu \bar\rho_\mu[\omega_\mu - v_\mu(\mathbf{r})]\psi_\mu^2(\mathbf{r})}{n(\mathbf{r})} - E_I. \tag{D9}$$

This expression can be transformed to a more transparent and computationally more convenient form by splitting $v_{\rm Hxc}^{\rm rc}$ in two parts:

$$v_{\rm Hxc}^{\rm rc}(\mathbf{r}) = v_{\rm xc}^{\rm resp}(\mathbf{r}) + v_{\rm Hxc}^{\rm cond}(\mathbf{r}), \tag{D10}$$

where

$$v_{\rm Hxc}^{\rm cond}(\mathbf{r}) = \frac{\sum_\mu \bar\rho_\mu \psi_\mu^2(\mathbf{r}) v_\mu(\mathbf{r})}{n(\mathbf{r})} \tag{D11}$$

and

$$v_{\rm xc}^{\rm resp}(\mathbf{r}) = -\frac{(\omega_1-\omega_0)\bar\rho_1\psi_1(\mathbf{r})^2}{n(\mathbf{r})} + E_G - \epsilon_g - \omega_0. \tag{D12}$$

In deriving the above equations, we used the definition of the density, Eq. (D5), and we set $E_I = \epsilon_g - E_G$ with ϵ_g denoting the one-particle ground-state energy.

Using the explicit expression of the potentials $v_\mu(\mathbf{r})$ [Eqs. (C7) and (C8)], we can eventually recast the "cond" term as

$$v_{\rm Hxc}^{\rm cond}(\mathbf{r}) = \frac{\sum_{\mu\nu}\sqrt{\bar\rho_\mu\bar\rho_\nu}\psi_\mu\psi_\nu\bar w_{\mu\nu}}{n(\mathbf{r})}. \tag{D13}$$

By a direct calculation one can then easily recover the expression of $v_{\rm Hxc}^{\rm cond}$ first obtained by Buijse *et al.* by a completely different method [55], namely, Eq. (19), with the two-particle density defined in Eq. (A6).

To arrive at the final expression for $v_{\rm xc}^{\rm resp}$, given in Eq. (18) we use the two following identities:

$$\omega_1 - \omega_0 = \bar h_{00} - \bar h_{11} \equiv -2t, \tag{D14}$$

$$E_G = \omega_0 + \bar h_{00} = 2\omega_0 - \langle\psi_0|v_0|\psi_0\rangle. \tag{D15}$$

Before coming to the proof of the above identities, let us note that Eq. (D14) implies that the optimized bonding orbital $|\psi_0\rangle$ corresponds to the highest Lagrange multiplier, i.e., $\omega_0 > \omega_1$, the opposite of the naive guess. This sign change is fundamental to obtain the correct behavior of $v_{\rm xc}^{\rm resp}$ and the correct decay of the density. The relation $\omega_0 > \omega_1$ indeed implies that the behavior of the density at large distances is governed by ω_0 that, as suggested by (D15), is correctly related to the ionization energy of the system [65]. Note, however, that within our approximations, ω_0 differs from the ionization energy by a small constant $\delta\epsilon_g = h_{00} - \epsilon_g$. The latter is due to the relaxation of the orbitals upon ionization and it tends to zero in the large-Z limit. By replacing Eqs. (D14) and (D15) in (D12), we arrive at the final expression for $v_{\rm xc}^{\rm resp}$ [Eq. (18)] and we can easily show that $\lim_{r\to\infty} v_{\rm xc}^{\rm resp}(\mathbf{r}) = \delta\epsilon_g$.

Equation (D14) can be proved by noting that from Eqs. (C6) it follows that

$$\omega_1 - \omega_0 = \bar h_{11} - \bar h_{00} + \langle\psi_1|v_1|\psi_1\rangle - \langle\psi_0|v_0|\psi_0\rangle, \tag{D16}$$

while from the definition of q and of the v_μ we have that

$$\langle\psi_1|v_1|\psi_1\rangle - \langle\psi_0|v_0|\psi_0\rangle = \bar w_{11,11} - \bar w_{00,00} - \frac{4\gamma\,\bar w_{01,01}}{1+\gamma^2} = 2(\bar h_{00} - \bar h_{11}), \tag{D17}$$

which replaced in Eq. (D16) leads to Eq. (D14). Notice that in the last step on the right-hand side of Eq. (D17) we have used the explicit expression of γ in terms of one- and two-electron integrals given in Eq. (A10).

In order to demonstrate Eq. (D15), we can start from the ground-state energy which can be recast in terms of the energies ω_i as follows:

$$E_G = \frac{1+q}{2}(\omega_0 + \bar h_{00}) + \frac{1-q}{2}(\omega_1 + \bar h_{11}), \tag{D18}$$

which using Eq. (D14) in turn leads to

$$E_G = \omega_0 + \bar h_{00} = \omega_1 + \bar h_{11}, \tag{D19}$$

which concludes the proof of Eq. (D15).

To obtain the L+REP results shown in the figures we replaced the bonding and antibonding states by appropriate linear combinations of atomic orbitals, i.e., we set

$$\psi_0(\mathbf{r}) = \frac{\varphi_{1s}(\mathbf{r}-\mathbf{R}_a) + \varphi_{1s}(\mathbf{r}-\mathbf{R}_b)}{\sqrt{2(1+S)}},$$
$$\psi_1(\mathbf{r}) = \frac{\varphi_{1s}(\mathbf{r}-\mathbf{R}_a) - \varphi_{1s}(\mathbf{r}-\mathbf{R}_b)}{\sqrt{2(1-S)}}, \tag{D20}$$

where $\varphi_{1s}(\mathbf{r}) = e^{-\xi|\mathbf{r}|}\sqrt{\xi^3/\pi}$, S denotes the overlap integral between $\varphi_{1s}(\mathbf{r}-\mathbf{R}_a)$ and $\varphi_{1s}(\mathbf{r}-\mathbf{R}_b)$, and ξ was obtained variationally.

In this way, we obtain

$$v_{\rm c}^{\rm kin}(0) = \frac{(1-q)}{2(1+q)}\frac{1+S}{1-S}\xi^2, \tag{D21}$$

$$v_{\rm Hxc}^{\rm cond}(0) = \frac{1}{2Z(1+S)}\int \frac{|\varphi_{1s}(\mathbf{r}-\mathbf{R}_a) + \varphi_{1s}(\mathbf{r}-\mathbf{R}_b)|^2}{|\mathbf{r}|}d\mathbf{r}. \tag{D22}$$

The integrals in $v_{\rm Hxc}^{\rm cond}$ are known [47]. For large Z (one-band limit), the crossover regime between strong and weak correlation lays at large separation a. Thus, we can set $S \simeq 0$ and $\xi = 1$, yielding Eqs. (20) and (21).

APPENDIX E: ORTHOGONALIZED ATOMIC ORBITALS

The optimized Wannier orbitals are approximated as

$$\phi_a(\mathbf{r}) = [\varphi_{1s}(\mathbf{r}-\mathbf{R}_a) - \alpha\,\varphi_{1s}(\mathbf{r}-\mathbf{R}_b)]/\sqrt{\mathcal{N}}, \tag{E1}$$

$$\phi_b(\mathbf{r}) = [\varphi_{1s}(\mathbf{r}-\mathbf{R}_b) - \alpha\,\varphi_{1s}(\mathbf{r}-\mathbf{R}_a)]/\sqrt{\mathcal{N}}, \tag{E2}$$

where $\alpha = (1-\sqrt{1-S^2})/S$ and $\mathcal{N} = (1-S^2)(1+\alpha^2)$.

The one- and two-center integrals defining the parameters of the generalized Hubbard model were calculated using the above approximate expressions for ϕ_a and ϕ_b. Within this approximation, the parameters $v = h_{aa}$, $t = -h_{ab}$, U, V, t_c, and K are then simply linear combination of the same parameters calculated with atomic orbitals which are exactly

known [47] (indicated with a tilde in the equations below). We have

$$
\begin{aligned}
v &= \frac{\tilde{v} + S\tilde{t}}{1 - S^2}, \\
t &= \frac{\tilde{t} + S\tilde{v}}{1 - S^2}, \\
U &= \frac{1}{2(1 - S^2)^2}[(2 - S^2)\tilde{U} - 4\tilde{t}_c S + S^2\tilde{V} + 2S^2\tilde{K}], \\
t_c &= \frac{1}{2(1 - S^2)^2}[2(1 + S^2)\tilde{t}_c - S(\tilde{U} + \tilde{V} + 2\tilde{K})], \\
V &= \frac{1}{2(1 - S^2)^2}[-4S\tilde{t}_c + 2\tilde{V} + S^2(\tilde{U} - \tilde{V} + 2\tilde{K})], \\
K &= \frac{1}{2(1 - S^2)^2}[-4S\tilde{t}_c + 2\tilde{K} + S^2(\tilde{U} + \tilde{V})],
\end{aligned}
$$

where we took $\tilde{K}' = \tilde{K}$.

APPENDIX F: WEAK SENSITIVITY OF THE REVERSE ENGINEERING POTENTIAL TO ORBITAL BASIS ERRORS

As explained above, the L+REP potential requires an inversion of the KS equation to obtain the noninteracting potential that yields a given correlated density. This task usually requires an extremely accurate basis to expand the wave functions and the density. Such large sensitivity of the potential is rooted in the presence of the Laplacian appearing in our case in Eq. (D8), leading to the "cond" and "resp" contributions while for the "kin" contribution the problem does not arise. To exemplify the problem, lets ψ_μ be molecular orbitals (MO) satisfying Eq. (C6) with v_μ set to zero and $\omega_0 = \epsilon_g$. Using these definitions, we can rewrite Eq. (D8) as

$$
v^{rc}_{\mathrm{Hxc}} = -\frac{t(1-q)2\psi_1^2(\mathbf{r})}{n(\mathbf{r})} + E_I - \epsilon_g \quad \text{(MO)}, \tag{F1}
$$

where all quantities should be evaluated in the MO basis. By comparing the above expression with Eqs. (18) and (19), we notice that (i) there is no "cond" contribution scaling as $1/(Z\,R)$; (ii) apart from constants Eq. (F1) resembles $v^{\mathrm{resp}}_{\mathrm{xc}}$ but it has the opposite sign. A different but still wrong result is obtained using in Eq. (D8) an approximated Gutzwiller density constructed using linear combinations of atomic orbitals. This extreme sensitivity problem is solved eliminating the Laplacian using a saddle condition for the energy and leading to Eqs. (17)–(19). Indeed, contrary to Eq. (F1), they reproduce one by one the equations of Ref. [55] simply evaluating their expressions in the same minimal basis we use.

Clearly, even using Eqs. (17)–(19) errors in the basis still will lead to errors in the potential, however, they can be shown to be quite mild in comparison with the errors which are incurred using equations containing the Laplacian. Indeed, $v^{\mathrm{kin}}_{\mathrm{xc}}(\mathbf{r})$ vanishes in the weak-coupling regime ($q \to 1$) while in the strong coupling it converges to the exact result in the Heitler-London limit ($q = 0$) obtained by Helbig *et al.* [53]. In the intermediate-coupling regime, it provides a smooth interpolation between these two extremes with the crossover at the right place in parameter space, ensuring that errors remain small.

As regards $v^{\mathrm{resp}}_{\mathrm{xc}}(\mathbf{r})$ we instead see that it is the sum of two parts: a spurious constant $\delta\epsilon_g$ (which by definition does not contribute to the barrier height) and a position-dependent potential which also does not contribute to the barrier height since it vanishes both at the origin and at infinity. The latter contribution is always quite small for homoatomic systems since the prefactor $(1 - q)t$ is small both in the weak and in the strong correlation limits. Notice that $\delta\epsilon_g$ would cancel in the approximation in which one uses the same orbitals to expand the two-site Hubbard model in the one- and two-electron cases.

The last contribution, $v^{\mathrm{cond}}_{\mathrm{Hxc}}(\mathbf{r})$, requires special care as it becomes numerically large for small Z and decays slow with distance. The two-particle density can be evaluated expanding the field operators in the minimal basis and using the lattice ground state to evaluate the two-body lattice density matrix. Fortunately, since there are no derivatives affecting the orbitals (and some are integrated), an extremely accurate knowledge of the orbitals is not required to obtain numerically accurate results.

We conclude saying that, while in principle ϕ_a and ϕ_b in Eqs. (17)-(19) are optimized Wannier orbitals whose shapes minimize the total energy, they can be safely replaced by approximate orbitals. In doing the plots, they were approximated with linear combinations of atomic $1s$ orbitals as defined in Appendix E.

APPENDIX G: MANY-SITE CASE

Analogously to the theory of superexchange [54], in the many-site case, we assume that in the strongly correlated limit on each bond the exchange-correlation potential has a structure which strongly resembles the one found in the diatomic molecule. As we did for the two-electron molecule, in the many-site many-electron case we therefore have to define an appropriate reference lattice model, find an appropriate single-particle basis set, and, after having estimated all parameters of the lattice model, calculate the one- and two-body densities.

As regards the first task, we start from the single-band generalized lattice model introduced in Eq. (A2) and, consistently with our assumptions concerning the potential, we truncate it neglecting three-site and interbond correlations. In this way, we essentially replicate the diatomic molecule Hamiltonian for each couple of sites present in the system and we obtain

$$
H_{1B} \simeq H_{\mathrm{chain}} \equiv U \sum_i n_{i\uparrow} n_{i\downarrow} - \varepsilon \sum_i n_i + \sum_{(i,j)} H^{\mathrm{bond}}_{i,j}, \tag{G1}
$$

where the sum over (i, j) is not limited to nearest-neighboring sites but include also next-to-nearest neighbors and we set

$$
\begin{aligned}
H^{\mathrm{bond}}_{ij} = & -t(c^\dagger_{i\sigma} c_{j\sigma} + \mathrm{H.c.}) + V n_i n_j \\
& + t_c \sum_\sigma (n_{i\bar{\sigma}} + n_{j\bar{\sigma}})(c^\dagger_{i\sigma} c_{j\sigma} + \mathrm{H.c.}) \\
& + K \sum_{\sigma\sigma'} c^\dagger_{i\sigma} c^\dagger_{j\sigma'} c_{i\sigma'} c_{j\sigma} + K' \sum_\sigma c^\dagger_{i\sigma} c^\dagger_{i\bar{\sigma}} c_{j\bar{\sigma}} c_{j\sigma}.
\end{aligned}
$$

In the above equation, the dependence of the matrix elements t, V, t_c, K, and K' on the distance $i - j$ is implied.

As regards the Wannier states, defining the optimum single-particle basis, we approximate them as linear combination of

atomic orbitals, similarly to what we did in the diatomic case. Namely, we assume that the Wannier orbital corresponding to site i equals a linear combination of atomic orbitals centered on the site i and on nearest- and next-nearest-neighboring sites and it can be written as follows:

$$\phi_i = \left(\varphi_i - \alpha \sum_u \varphi_{i+u} - \beta \sum_v \varphi_{i+v}\right) \Big/ \sqrt{\mathcal{N}}, \qquad \text{(G2)}$$

where u and v implement translations, respectively, on nearest- and next-nearest-neighboring sites and the weights α and β and the normalization $\mathcal{N}$ are determined imposing orthonormality.

Using the above equation, as in the diatomic case, we express all integrals appearing in the potentials and the different parameters appearing in the lattice Hamiltonian as linear combinations of known two-center integrals involving Slater orbitals and we calculate them analytically. Once this is done, we determine the ground state of H_{chain} by exact diagonalization and we calculate the hopping reduction factor q and the two-body density matrix on the lattice needed to finally estimate the potential by simply generalizing Eqs. (17)–(19) as explained in the main text.

APPENDIX H: QUANTUM CHEMISTRY COMPUTATIONS

Accurate densities in Fig. 3 were obtained using full CI with the ORCA computer code [67]. Very large basis sets were used in order to have well-converged densities. In particular, we used the fully uncontracted aug-mcc-pV8Z [68] for the case $Z = 1$ and the same basis set with the exponent appropriately scaled for the systems with $Z > 1$.

Accurate Kohn-Sham potentials used as reference in Figs. 5, 7, and 6 were extracted by using Eq. (D3) starting from the full CI densities obtained as above. The density was computed on a cubic grid and spurious features in the KS potential due to the basis set were removed by applying the scheme described in Ref. [64]. For the four-site case [Fig. 8(b)] full CI is not feasible. Therefore, we used the coupled cluster method using aug-cc-pV5Z basis set with the code ORCA [67].

The LDA potentials and noninteracting densities were calculated using CP2K code [43].

[1] W. Kohn, Rev. Mod. Phys. **71**, 1253 (1999).
[2] W. Kohn and L. J. Sham, Phys. Rev. **140**, A1133 (1965).
[3] A. D. Becke, Phys. Rev. A **38**, 3098 (1988).
[4] J. P. Perdew, K. Burke, and M. Ernzerhof, Phys. Rev. Lett. **77**, 3865 (1996).
[5] A. D. Becke, J. Chem. Phys. **98**, 5648 (1993).
[6] Jianwei Sun, Bing Xiao, Yuan Fang, Robin Haunschild, Pan Hao, Adrienn Ruzsinszky, Gbor I. Csonka, Gustavo E. Scuseria, and John P. Perdew, Phys. Rev. Lett. **111**, 106401 (2013).
[7] Jianwei Sun, Adrienn Ruzsinszky, and John P. Perdew, Phys. Rev. Lett. **115**, 036402 (2015).
[8] F. Della Sala, E. Fabiano, and L. A. Constantin, Phys. Rev. B **91**, 035126 (2015).
[9] L. A. Constantin, E. Fabiano, J. M. Pitarke, and F. Della Sala, Phys. Rev. B **93**, 115127 (2016).
[10] V. U. Nazarov and G. Vignale, Phys. Rev. Lett. **107**, 216402 (2011).
[11] N. F. Mott, Proc. Phys. Soc. London, Sect. A **62**, 416 (1949).
[12] M. Imada, A. Fujimori, and Y. Tokura, Rev. Mod. Phys. **70**, 1039 (1998).
[13] P. Coleman, in *Handb. Magn. Adv. Magn. Mater. Handb. Magn. Adv. Magn. Mater. Vol 1 Fundam. Theory*, edited by Helmut Kronmuller and Stuart Parkin (Wiley, Hoboken, NJ, 2006), pp. 95–148.
[14] J. Rusz, P. M. Oppeneer, N. J. Curro, R. R. Urbano, B.-L. Young, S. Lebègue, P. G. Pagliuso, L. D. Pham, E. D. Bauer, J. L. Sarrao, and Z. Fisk, Phys. Rev. B **77**, 245124 (2008).
[15] M. Grüning, O. V. Gritsenko, and E. J. Baerends, J. Chem. Phys. **118**, 7183 (2003).
[16] O. V. Gritsenko and E. J. Baerends, Theor. Chem. Acc. **96**, 44 (1997).
[17] J. P. Perdew, A. Savin, and K. Burke, Phys. Rev. A **51**, 4531 (1995).
[18] M. A. Kastner, R. J. Birgeneau, G. Shirane, and Y. Endoh, Rev. Mod. Phys. **70**, 897 (1998).
[19] J. M. Luttinger, Phys. Rev. **119**, 1153 (1960).
[20] G. Kotliar, S. Y. Savrasov, K. Haule, V. S. Oudovenko, O. Parcollet, and C. A. Marianetti, Rev. Mod. Phys. **78**, 865 (2006).
[21] J. Hubbard, Proc. R. Soc. London, Sect. A **276**, 238 (1963).
[22] M. C. Gutzwiller, Phys. Rev. Lett. **10**, 159 (1963).
[23] J. Kanamori, Prog. Theor. Phys. **30**, 275 (1963).
[24] A. Georges, G. Kotliar, W. Krauth, and M. J. Rozenberg, Rev. Mod. Phys. **68**, 13 (1996).
[25] V. I. Anisimov, J. Zaanen, and O. K. Andersen, Phys. Rev. B **44**, 943 (1991).
[26] J. Bünemann, F. Gebhard, and W. Weber, in *Frontiers in Magnetic Materials*, edited by A. V. Narlikar (Springer, Berlin, 2005), Vol. 4, p. 117.
[27] G.-T. Wang, X. Dai, and Z. Fang, Phys. Rev. Lett. **101**, 066403 (2008).
[28] K. M. Ho, J. Schmalian, and C. Z. Wang, Phys. Rev. B **77**, 073101 (2008).
[29] Y. X. Yao, J. Schmalian, C. Z. Wang, K. M. Ho, and G. Kotliar, Phys. Rev. B **84**, 245112 (2011).
[30] R. M. Martin, *Electronic Structure: Basic Theory and Practical Methods* (Cambridge University Press, Cambridge, 2008), pp. 1–647.
[31] C. A. Ullrich and W. Kohn, Phys. Rev. Lett. **87**, 093001 (2001).
[32] W. F. Brinkman and T. M. Rice, Phys. Rev. B **2**, 4302 (1970).
[33] W. Metzner and D. Vollhardt, Phys. Rev. B **37**, 7382 (1988).
[34] F. Gebhard, Phys. Rev. B **41**, 9452 (1990).
[35] E. Dagotto, Rev. Mod. Phys. **66**, 763 (1994).
[36] A. Kramida, Yu. Ralchenko, J. Reader, and NIST ASD Team, *NIST Atomic Spectra Database (version 5.1)* (National Institute of Standards and Technology, Gaithersburg, MD, 2013).
[37] J. C. Amadon and J. E. Hirsch, Phys. Rev. B **54**, 6364 (1996).
[38] J. Spałek, R. Podsiadły, W. Wójcik, and A. Rycerz, Phys. Rev. B **61**, 15676 (2000).
[39] Valentina Brosco, Zu-Jian Ying, and J. Lorenzana (unpublished).
[40] D. Vollhardt, Rev. Mod. Phys. **56**, 99 (1984).

[41] M. Karski, C. Raas, and G. S. Uhrig, Phys. Rev. B **72**, 113110 (2005).
[42] N. Blümer and E. Kalinowski, Phys. Rev. B **71**, 195102 (2005).
[43] J. VandeVondele, M. Krack, F. Mohamed, M. Parrinello, T. Chassaing, and J. Hutter, Comput. Phys. Commun. **167**, 103 (2005).
[44] P. R. T. Schipper, O. V. Gritsenko, and E. J. Baerends, Theor. Chem. Acc. **99**, 329 (1998).
[45] A. Savin, F. Colonna, and R. Pollet, Int. J. Quantum Chem. **93**, 166 (2003).
[46] E. Fabiano and L. A. Constantin, Phys. Rev. A **87**, 012511 (2013).
[47] J. C. Slater, *Quantum Theory of Molecules and Solids Vol. 1* (McGraw-Hill, New York, 1965).
[48] J. P. Perdew, in *Density Functional Methods in Physics*, edited by R. M. Dreizler and J. da Providencia (Springer, Boston, 1985), pp. 265–308.
[49] R. van Leeuwen, O. Gritsenko, and E. J. Baerends, Z. Phys. D **33**, 229 (1995).
[50] O. V. Gritsenko, R. van Leeuwen, and E. J. Baerends, J. Chem. Phys. **104**, 8535 (1996).
[51] R. van Leeuwen, O. V. Gritsenko, and E. J. Baerends, in *Density Functional Theory I*, Vol. 180 of Topics in Current Chemistry, edited by R. F. Nalewajski (Springer, Berlin, 1996), pp. 107–167.
[52] O. V. Gritsenko, B. Ensing, P. R. T. Schipper, and E. J. Baerends, J. Phys. Chem. A **104**, 8558 (2000).
[53] N. Helbig, I. V. Tokatly, and A. Rubio, J. Chem. Phys. **131**, 224105 (2009).
[54] P. Anderson, Phys. Rev. **79**, 350 (1950).
[55] M. A. Buijse, E. J. Baerends, and J. G. Snijders, Phys. Rev. A **40**, 4190 (1989).
[56] R. van Leeuwen and E. J. Baerends, Int. J. Quantum Chem. **52**, 711 (1994).
[57] J. P. Perdew, Phys. Rev. B **33**, 8822 (1986).
[58] A. J. Cohen, P. Mori-Sánchez, and W. Yang, Science **321**, 792 (2008).
[59] W. Metzner and D. Vollhardt, Phys. Rev. Lett. **59**, 121 (1987).
[60] G. Buttazzo, L. De Pascale, and P. Gori-Giorgi, Phys. Rev. A **85**, 062502 (2012).
[61] F. Malet, A. Mirtschink, K. Giesbertz, L. Wagner, and P. Gori-Giorgi, Phys. Chem. Chem. Phys. **16**, 14551 (2014).
[62] J. P. Perdew and Y. Wang, Phys. Rev. B **45**, 13244 (1992).
[63] R. van Leeuwen and E. J. Baerends, Phys. Rev. A **49**, 2421 (1994).
[64] A. P. Gaiduk, I. G. Ryabinkin, and V. N. Staroverov, J. Chem. Theory Comput. **9**, 3959 (2013).
[65] C. O. Almbladh and U. von Barth, Phys. Rev. B **31**, 3231 (1985).
[66] M. Levy, J. P. Perdew, and V. Sahni, Phys. Rev. A **30**, 2745 (1984).
[67] F. Neese, Wiley Interdiscip. Rev.: Comput. Mol. Sci. **2**, 73 (2012).
[68] S. L. Mielke, D. W. Schwenke, and K. A. Peterson, J. Chem. Phys. **122**, 224313 (2005).